JEM Journal of Experimental Medicine

BRIEF DEFINITIVE REPORT

Ganglioneuromas are driven by activated AKT and can be therapeutically targeted with mTOR inhibitors

Ting Tao[1*], Hui Shi[1*], Meng Wang[2], Antonio R. Perez-Atayde[3], Wendy B. London[1,4], Alejandro Gutierrez[1,4], Bernardo Lemos[2], Adam D. Durbin[1,4,5**], and A. Thomas Look[1**]

Peripheral sympathetic nervous system tumors are the most common extracranial solid tumors of childhood and include neuroblastoma, ganglioneuroblastoma, and ganglioneuroma. Surgery is the only effective therapy for ganglioneuroma, which may be challenging due to the location of the tumor and involvement of surrounding structures. Thus, there is a need for well-tolerated presurgical therapies that could reduce the size and extent of ganglioneuroma and therefore limit surgical morbidity. Here, we found that an AKT–mTOR–S6 pathway was active in human ganglioneuroma but not neuroblastoma samples. Zebrafish transgenic for constitutively activated *myr-Akt2* in the sympathetic nervous system were found to develop ganglioneuroma without progression to neuroblastoma. Inhibition of the downstream AKT target, mTOR, in zebrafish with ganglioneuroma effectively reduced the tumor burden. Our results implicate activated AKT as a tumorigenic driver in ganglioneuroma. We propose a clinical trial of mTOR inhibitors as a means to shrink large ganglioneuromas before resection in order to reduce surgical morbidity.

Introduction

Peripheral sympathetic nervous system (PSNS) tumors are one of the most common solid tumors of childhood other than brain tumors (Shohet and Foster, 2017). These tumors are classified into several basic categories, each with several subtypes: neuroblastoma (undifferentiated, poorly differentiated, and differentiating), ganglioneuroblastoma (intermixed and nodular), and ganglioneuroma (maturing and mature; Shimada et al., 1999a, 1999b; Shimada and Ambros, 2005). Neuroblastoma is the most malignant and immature category of these tumors and accounts for 15% of childhood cancer deaths (Cheung and Dyer, 2013; Matthay et al., 2016). Ganglioneuroma is a nonmalignant tumor made up of differentiated gangliocytes and mature stroma. Ganglioneuroblastoma contains immature neuroblasts that grow and migrate abnormally, similar to neuroblastoma, as well as more mature tissues that are similar to ganglioneuroma (Lonergan et al., 2002). An effective management strategy for ganglioneuroblastoma and ganglioneuroma is surgery, although these tumors are frequently large, encasing and compressing surrounding major vessels and nerves, including the spinal cord, resulting in difficult surgical resection with significant postoperative morbidities (Retrosi et al., 2011). To date, no drugs are available that demonstrate a reduction in mature neuroblastic tumor burden (Decarolis et al., 2016).

The genetics of neuroblastoma have been extensively profiled. *MYCN* gene amplification is found in ∼20% of neuroblastomas and is a well-established indicator of high-risk disease and a poor prognosis (Huang and Weiss, 2013). Further, overexpression of MYCN or c-MYC in the PSNS of mouse or zebrafish models induces neuroblastoma in the sympathetic ganglia or adrenal/interrenal medulla, highly resembling human neuroblastoma (Tao et al., 2017; Weiss et al., 1997; Zimmerman et al., 2018; Zhu et al., 2012). In contrast, little is known about the genetics of mature ganglioneuroma. Type 2B multiple endocrine neoplasia patients with activating germline RET oncogene mutations may rarely develop ganglioneuroma (Lora et al., 2005; Yamasaki et al., 2017). Overexpression of the activated RET proto-oncogene RET^{M918T} (Sweetser et al.,

[1]Department of Pediatric Oncology, Dana-Farber Cancer Institute, Harvard Medical School, Boston, MA; [2]Department of Environmental Health & Molecular and Integrative Physiological Sciences Program, Harvard T.H. Chan School of Public Health, Boston, MA; [3]Department of Pathology, Boston Children's Hospital, Harvard Medical School, Boston, MA; [4]Division of Hematology/Oncology, Boston Children's Hospital, Harvard Medical School, Boston, MA; [5]The Broad Institute of MIT and Harvard, Cambridge, MA.

*T. Tao and H. Shi contributed equally to this paper; **A.T. Look and A.D. Durbin contributed equally to this paper; Correspondence to A. Thomas Look: thomas_look@dfci.harvard.edu; Adam D. Durbin: adam_durbin@dfci.harvard.edu; Ting Tao: ting_tao@dfci.harvard.edu.

1999) or activated Ras (Sweetser et al., 1997) in the PSNS of mice results in neuroglial tumors or ganglioneuroma. Further, deletion of *Pten* in the mouse enteric nervous system results in increased activity of the phosphatidylinositol 3-kinase (PI3K)/PTEN–AKT–mTOR–S6K signaling pathway and causes ganglioneuromatosis with chronic intestinal pseudoobstruction (Puig et al., 2009). Ganglioneuroma is rarely associated with other human syndromes, including neurofibromatosis type 1 (Abdulkader et al., 2016), congenital central hypoventilation syndrome (Trochet et al., 2004), and ROHHAD syndrome (Maksoud and Kassab, 2015). Aside from studies in animal models and the rare associations with genetic diseases in humans, the etiology and molecular basis for childhood ganglioneuroma remain elusive.

The PI3K–AKT–mTOR pathway is a pivotal regulator of cellular activities including cell growth and apoptosis (Vanhaesebroeck et al., 2012). Aberrant activation of the PI3K–AKT pathway has been observed in various human tumors including breast cancer, colorectal cancer, and squamous cell lung carcinoma. As a serine-threonine kinase, AKT serves as an attractive therapeutic target (Alexander, 2011; Engelman, 2009). One classically implicated key target of AKT is the mTOR protein kinase that regulates downstream cell growth, viability, and survival (Manning and Toker, 2017; Saxton and Sabatini, 2017). Inhibition of AKT–mTOR signaling is of significant clinical interest, and mTOR inhibition with sirolimus or related drugs has been key to management of the genetic disease tuberous sclerosis, in which treatment of mature subependymal giant cell astrocytomas with mTOR inhibitors results in sustained clinical benefit in pediatric patients (Jeong and Wong, 2016; Rosset et al., 2017).

Here, we found that phosphorylated, activated AKT and the downstream effectors mTOR and ribosomal protein S6 were more frequently detected in human primary ganglioneuromas than in poorly differentiated human neuroblastomas. To test whether activated AKT is sufficient to drive tumorigenesis in ganglioneuroma, we generated a transgenic zebrafish model in which a constitutively active, myristoylated murine Akt2 (myr-Akt2; Tan et al., 2008) is expressed in the PSNS driven by the zebrafish *dopamine-β-hydroxylase* (*dβh*) gene promoter (Zhu et al., 2012). Overexpression of myr-Akt2 led to the development of ganglioneuroma in the interrenal gland (IRG), the zebrafish equivalent of human adrenal gland, that closely resembles human ganglioneuroma. Mechanistically, myr-Akt2 overexpression induced sympathoadrenal lineage hyperplasia through increased cell proliferation, concurrent with activation of the AKT target mTOR. The mTOR inhibitors sirolimus and everolimus effectively reduced tumor burden in zebrafish with ganglioneuroma. Thus, our data unexpectedly reveal that activated AKT is both necessary and sufficient to drive the formation of ganglioneuroma, and we propose that mTOR inhibitors like sirolimus and everolimus are ideal drugs to test in clinical trials designed to reduce ganglioneuroma burden in patients before surgical resection as a means to reduce patient morbidity.

Results and discussion

Phosphorylated AKT expression in primary childhood ganglioneuromas and neuroblastomas

To understand the contribution of AKT to human primary neuroblastic tumors, we performed immunohistochemistry (IHC) for phosphorylated AKT on a panel of human primary ganglioneuromas (including two ganglioneuroblastoma samples) and compared these results with those from human primary neuroblastomas using two-sided Fisher's exact tests. These data revealed that 10 of 11 ganglioneuromas (90.91%; 95% confidence interval [CI; 58.72% to 99.77%]) expressed moderate to high levels of activated, phosphorylated AKT (Ser473), while only 1 of 15 poorly differentiated neuroblastomas (6.67%; 95% CI [1.70% to 31.95%]) expressed detectable phosphorylated AKT (Ser473; $P < 0.0001$; Fig. 1). However, each of the ganglioneuromas and 14 of 15 neuroblastomas were positive for pan-AKT by IHC ($P = 1$; Fig. 1). To further confirm the activation of the AKT pathway in ganglioneuromas, we performed additional IHC against downstream targets in the AKT pathway. We found that phosphorylated mTOR (Ser2448) was expressed in 9 of 11 ganglioneuromas (81.82%; 95% CI [48.22% to 97.72%]) but only in 5 of 15 poorly differentiated neuroblastomas (33.33%; 95% CI [11.82% to

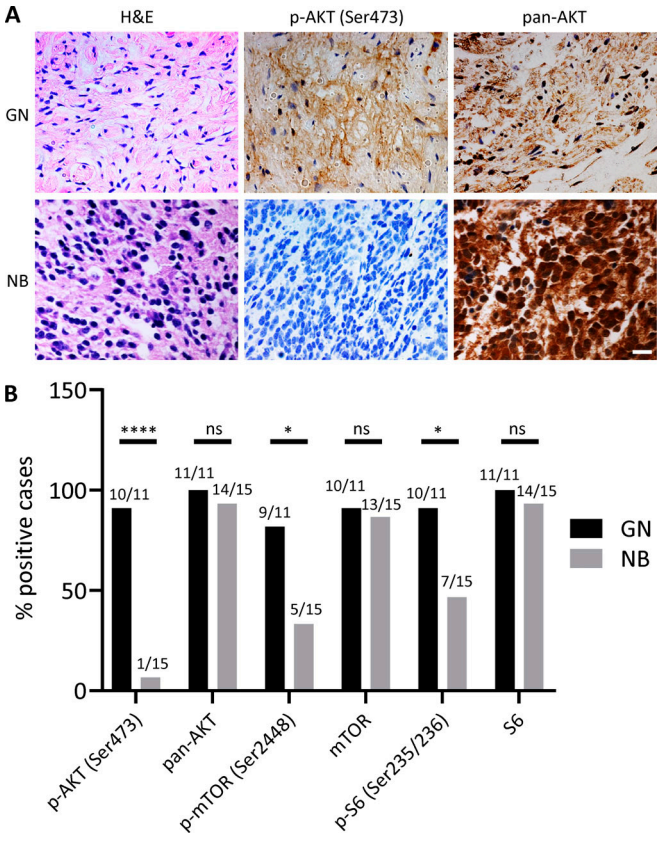

Figure 1. **Immunohistochemical evaluation of AKT and its downstream target proteins phosphorylation in human primary ganglioneuroma and poorly differentiated neuroblastoma samples. (A)** H&E staining and IHC with phosphorylated AKT (p-AKT; Ser473) and pan-AKT for a representative human primary ganglioneuroma (GN) and poorly differentiated neuroblastoma (NB). Scale bar, 20 µm. Protein expression is indicated by brown staining. **(B)** The percentage of p-AKT (Ser473), pan-AKT, phosphorylated mTOR (p-mTOR; Ser2448), mTOR, phosphorylated S6 ribosomal protein (p-S6; Ser235/236), and S6-positive cases in GN and NB. The number of positive and total cases is indicated on top of each column. The significance of the ratios of positive to negative tumors by IHC for these target proteins between GN and NB were determined by two-sided Fisher's exact test. ns, not significant; *, $P < 0.05$; ****, $P < 0.0001$.

61.62%]; P = 0.0214; Fig. 1 B and Fig. S1 A). Similarly, phosphorylated S6 ribosomal protein (Ser235/236) was expressed in 10 of 11 ganglioneuromas (90.91%; 95% CI [58.72% to 99.77%]) but only in 7 of 15 poorly differentiated neuroblastomas (46.67%; 95% CI [21.27% to 73.41%]; P = 0.0362; Fig. 1 B and Fig. S1 B). 10 of 11 ganglioneuromas and 13 of 15 neuroblastomas were positive for total mTOR expression (P = 1; Fig. 1 B and Fig. S1 A), and each of the ganglioneuromas and 14 of 15 neuroblastomas were positive for total S6 protein expression (P = 1; Fig. 1 B and Fig. S1 B). The demographic characteristics of patient samples used in this study are presented as Table S1. These data support the hypothesis that AKT and its downstream targets, mTOR and S6, are frequently activated in differentiated human primary ganglioneuromas and less activated in poorly differentiated neuroblastomas, and therefore implicate activated AKT as important in the pathogenesis of ganglioneuroma, but not neuroblastoma.

Activated AKT is sufficient to produce ganglioneuroma in zebrafish

AKT activation in ganglioneuromas does not necessarily implicate it as a driver of this tumor, because it might be activated as consequence rather than a cause of aberrant growth. To test whether activated AKT is important in the initiation of ganglioneuroma, we generated stable transgenic zebrafish lines that coexpress *mCherry* and a constitutively active *myr-Akt2* (Tan et al., 2008) in the PSNS under control of the zebrafish *dβh* promoter (Zhu et al., 2012). Two independent transgenic lines were established: *Tg(dβh:mCherry;dβh:myr-Akt2)* #1 and #2, here designated myr-Akt2#1 and #2. A previously established *Tg(dβh:mCherry)* line (designated mCherry; Zhu et al., 2017) was used as a control. Each line was maintained by crossing heterozygous fish with wild-type AB fish, and progeny were identified that expressed mCherry in the superior cervical ganglia at 3 d postfertilization (dpf). In both myr-Akt2 lines, mCherry-positive tumor masses were visualized in the anterior abdomen, arising in the IRG, under a stereo fluorescence dissecting microscope (Fig. 2, A and D). Histopathological analyses revealed that these tumors were ganglioneuromas and composed of differentiated, mature ganglion cells with poor Schwannian stroma (Fig. 2, B, C, E, and F), which were clearly distinguishable from MYCN-induced neuroblastomas (Fig. 2, G–I) that arose in our previously described zebrafish neuroblastoma model *Tg (dβh:EGFP-MYCN)* (designated MYCN; Zhu et al., 2012). Fish transgenic for *myr-Akt2* developed mCherry-positive ganglioneuromas in the IRG starting at 13 wk postfertilization (wpf) with a penetrance of 40–50% by 29 wpf (P = 0.0003 and P < 0.0001 for myr-Akt2#1 and #2 compared with the complete lack of tumors in the control mCherry line; Fig. 2 J). By comparison, fish transgenic for *MYCN* developed EGFP-positive neuroblastomas in the IRG starting at 7 wpf with a penetrance of ∼40% by 29 wpf (P < 0.0001 compared with the complete lack of tumors in the control mCherry line; Fig. 2 J).

While pan-Akt protein expression was detected in normal head kidney and tumors of each genotype (Fig. S2, B, G, and L), phosphorylated Akt (Ser473) expression was only detected in myr-Akt2 transgenic tumors (Fig. S2, A, F, and K). Normal cells of the IRG in the control mCherry fish were predominately differentiated chromaffin cells and expressed tyrosine hydroxylase (TH), as did tumor cells of each genotype (Fig. S2, C, H, and M). The tumor cells, but not normal chromaffin cells in the IRG, were positive for the tumor makers Hu-Antigen C (HuC) and Synaptophysin (Fig. S2, D, E, I, J, N, and O), indicating that tumor cells retained neural markers and arose from sympathetic neuroblasts, but not chromaffin cells.

AKT signaling has been shown to drive both cell survival and proliferation (Irie et al., 2005), and functions as an intermediate between the upstream receptor tyrosine kinase–PI3K signaling and numerous downstream effectors (Manning and Toker, 2017). Since human tumors displayed activation of the mTOR-S6 signaling axis downstream of AKT (Fig. 1), we hypothesized that constitutively active myr-Akt2 might result in activation of similar mTOR signaling during ganglioneuroma tumorigenesis. Immunohistochemical analysis of tumor sections revealed high level expression of phosphorylated mTOR (Ser2448) and the mTOR targets S6 ribosomal protein (Ser235/236) and EIF4EBP1 (Thr37/46) in myr-Akt2 tumors, whereas levels of phosphorylated mTOR (Ser2448) and S6 ribosomal protein (Ser235/236) were undetectable in MYCN-induced neuroblastomas (Fig. S2, P–X). These data indicate that activation of the mTOR signaling pathway is associated with myr-Akt2–driven mature ganglioneuroma, but not MYCN-driven highly malignant neuroblastoma.

Activated AKT induces sympathoadrenal cell proliferation to drive ganglioneuroma formation

Previous studies showed that overexpression of MYCN-induced sympathoadrenal cells hyperplasia in our neuroblastoma model (Zhu et al., 2012). In our current study, we use the same approach to identify the effects of myr-Akt2 on these cells during ganglioneuroma pathogenesis. All the fish used in this analysis were in the *Tg(dβh:EGFP)* (designated EGFP) background. We examined the numbers of EGFP$^+$ sympathoadrenal cells in the sections of the IRG region of different transgenic lines. The numbers of EGFP$^+$ sympathoadrenal cells were significantly increased in the myr-Akt2;EGFP line, as compared with those in the control EGFP line at 5 wpf (Fig. 3). Similarly, MYCN;EGFP transgenic fish also showed increased numbers of EGFP$^+$ sympathoadrenal cells in the IRG relative to the EGFP line (Fig. 3). Using 5-ethynyl-2′-deoxyuridine (EdU) labeling to determine the proliferative fraction of the sympathoadrenal cells in the IRG region of the myr-Akt2;EGFP line, we found that 0.77% of the EGFP$^+$ sympathoadrenal cells showed incorporation of EdU after 2 h of pulse labeling, with no EdU$^+$ sympathoadrenal cells identified in control EGFP line (P = 0.0108; Fig. S3, A–J). MYCN;EGFP transgenic line exhibited even higher percentages of EdU$^+$ sympathoadrenal cells (5.83%, P < 0.0001 versus control EGFP line; Fig. S3, A–J) due to the proliferative signals from overexpression of MYCN. Thus, AKT activation caused a modest increase in cell proliferation of ganglioneuroma, which although much less than that induced by MYCN in neuroblastoma nevertheless resulted in sympathoadrenal lineage cell hyperplasia, as reflected by the appearance of low-grade ganglioneuroma in transgenic zebrafish.

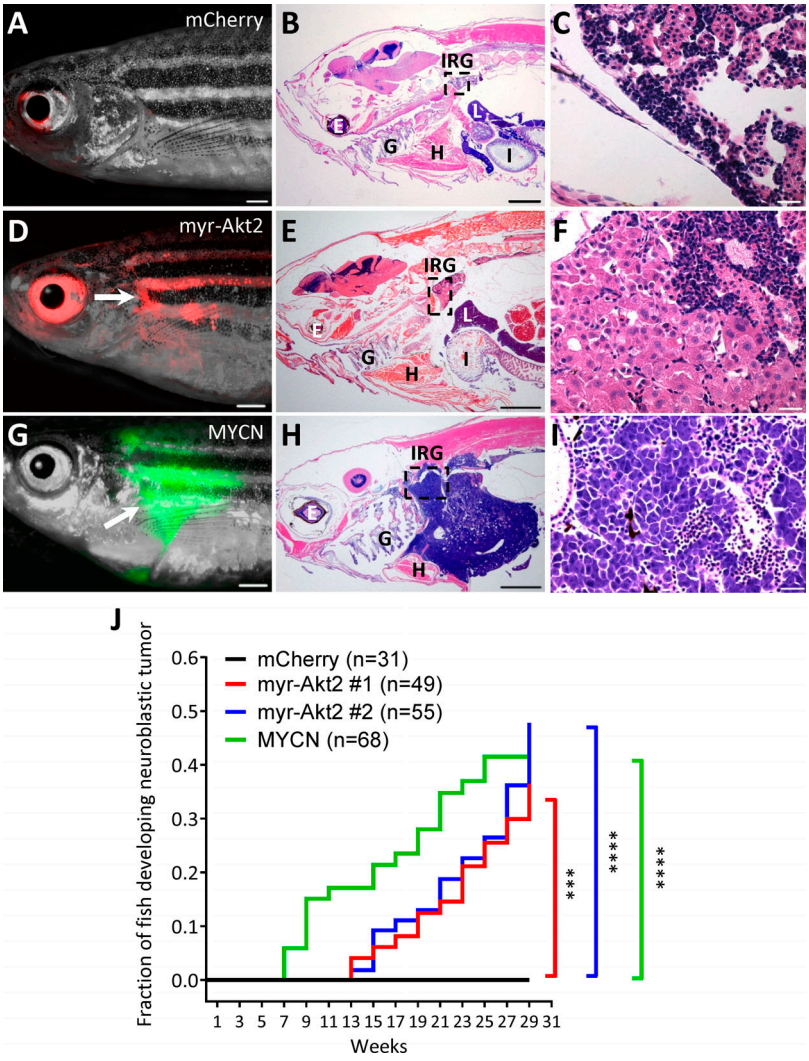

Figure 2. **Ganglioneuromas arise in myr-Akt2–expressing transgenic zebrafish. (A–I)** Images of a 25 wpf control mCherry transgenic line without detectable mCherry-positive tumor in the IRG (A), a 25 wpf myr-Akt2 transgenic line with mCherry-positive ganglioneuroma (arrow) arising in the IRG (D), and a 20 wpf MYCN transgenic line with EGFP-positive neuroblastoma (arrow) arising in the IRG (G). Scale bars represent 1 mm for A, D, and G. H&E-stained sagittal sections of mCherry transgenic line (B and C), myr-Akt2 transgenic line with ganglioneuroma (E and F), and MYCN transgenic line with neuroblastoma (H and I). Boxes in B, E, and H indicate the IRG and are magnified in C, F, and I, respectively. E, eye; G, gill; H, heart; I, intestine; L, liver. Scale bars represent 1 mm for B, E, and H and 20 µm for C, F, and I. **(J)** Cumulative frequency of ganglioneuromas in two independent myr-Akt2 stable transgenic zebrafish lines and a MYCN transgenic zebrafish line by Kaplan–Meier analysis. The difference between tumor onset by 29 wpf for myr-Akt2#1, myr-Akt2#2, and MYCN versus mCherry transgenic fish was determined by two-sided log-rank test. ***, $P < 0.001$; ****, $P < 0.0001$.

Zebrafish ganglioneuroma and neuroblastoma recapitulate the gene expression patterns of their respective human tumors

Ganglioneuroma and neuroblastoma both originate from migratory PSNS neuroblasts, representing benign and malignant tumors arising from the same progenitor cell lineage. We next sought to identify gene expression signatures that distinguished between ganglioneuroma and neuroblastoma. RNA sequencing (RNA-seq) was performed using zebrafish ganglioneuroma and neuroblastoma cells that were isolated by FACS-sorting from myr-Akt2 and MYCN fish, respectively (Fig. 4 A). Published microarray data for human ganglioneuromas and neuroblastomas (Albino et al., 2008) were analyzed to determine whether zebrafish tumors resembled human tumors at the levels of gene expression.

By performing gene set enrichment analysis (GSEA), we found that the PI3K pathway is up-regulated in both human and zebrafish ganglioneuromas when compared with neuroblastoma samples, consistent with the activation of AKT in ganglioneuroma (Fig. 4 B). Further analyses were based on the 4,321 Biomart "one-to-one" orthologous genes between human and zebrafish (Table S2). Analysis of 407 differentially expressed genes with absolute $\log_2$-fold-difference >1 in ganglioneuromas compared with neuroblastomas showed coordinate differences in gene expression in both human and zebrafish tumors (Pearson's $r = 0.39$, $P < 2.2 \times 10^{-16}$), with 282 genes (69.3%) co-upregulated or co-down-regulated (Fig. 4 C). Among the top 20 down- or up-regulated genes, we noted down-regulation in both human and zebrafish ganglioneuromas of the adrenergic core regulatory circuit (CRC) transcription factors that were recently described by ours and other groups (Boeva et al., 2017; Durbin et al., 2018; van Groningen et al., 2017), including *TFAP2B*, *ISL1*, *GATA3*, *PHOX2A*, and *PHOX2B* (Fig. 4 D). Thus, this critical CRC driving the adrenergic subtype of neuroblastoma is not active in low-grade ganglioneuroma. By contrast, other transcription factors were highly expressed in both human and zebrafish ganglioneuroma samples, including the key neural crest transcription factor *SOX10*, but down-regulated in neuroblastomas (Fig. 4 D). Thus, the ganglioneuroma developed in our zebrafish model resembles human ganglioneuroma, both histologically and by gene expression.

mTOR inhibitors target ganglioneuroma cells

Our finding that activated AKT pathways drive ganglioneuroma formation in zebrafish and can be prominently detected in

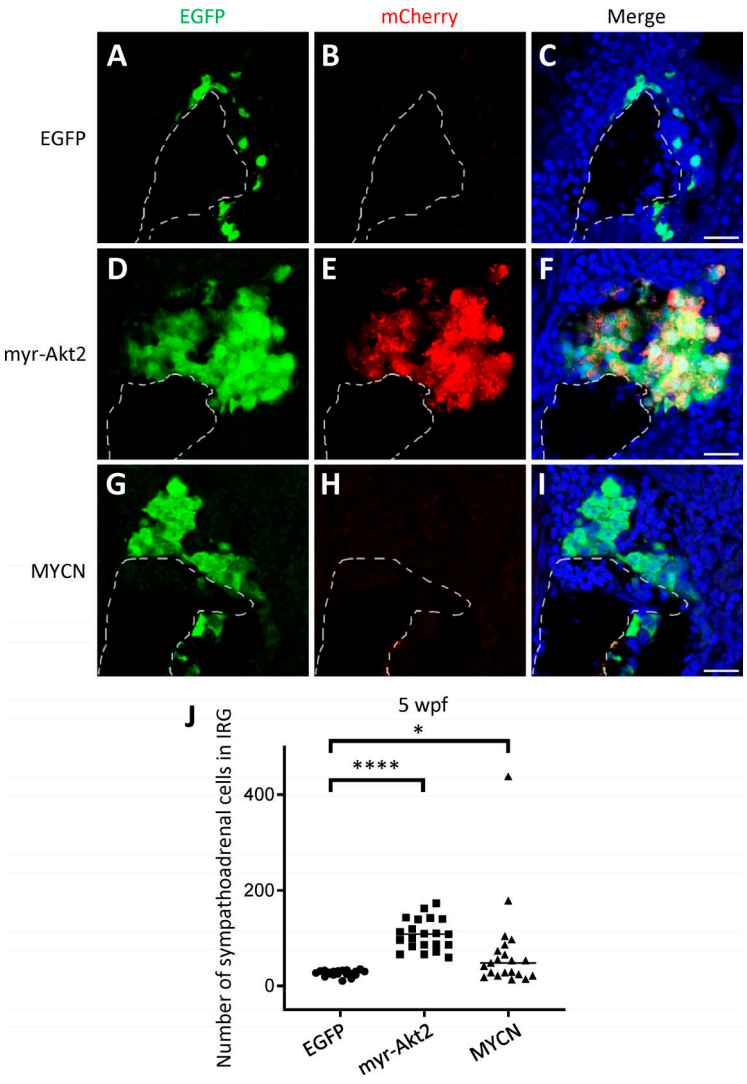

Figure 3. **myr-Akt2 causes sympathoadrenal lineage cells hyperplasia in the IRG at 5 wpf. (A–I)** Representative coimmunostaining images of EGFP and mCherry of the sagittal sections through IRG of EGFP (A–C), myr-Akt2;EGFP (D–F), and MYCN;EGFP (G–I) transgenic lines at 5 wpf. Nuclei were stained with DAPI. Dotted lines indicate the head kidney (HK) boundary. Scale bar, 20 µm. **(J)** Numbers of EGFP$^+$ sympathoadrenal cells in the IRG of control EGFP, myr-Akt2;EGFP, and MYCN;EGFP transgenic fish at 5 wpf. Each symbol represents the value for an individual fish. Horizontal bars indicate medians that were compared with two-tailed Wilcoxon rank-sum test. *, $P < 0.05$; ****, $P < 0.0001$.

childhood ganglioneuroma raised the possibility that these tumors might be sensitive to inhibitors of pathways downstream of AKT. Ganglioneuromas are primarily treated by surgical resection, but can be large in size and are often intimately associated with vasculature and neuronal bundles. For these reasons, surgical resection can be associated with significant morbidity in the setting of large or difficult to resect tumors (Table S3; Alexander et al., 2018; Retrosi et al., 2011). In these patients, it would be desirable to reduce the size and extent of the tumor before surgery. Unfortunately, chemotherapeutic agents have not yet been identified that show efficacy in these tumors (Decarolis et al., 2016).

Based on our findings implicating activated AKT and downstream signaling through mTOR and S6, we reasoned that ganglioneuroma might be sensitive to the inhibition of the mTOR kinase. In our zebrafish model, primary zebrafish ganglioneuroma cells were isolated from the myr-Akt2 tumor-bearing fish and transplanted into the pericardial cavity of casper recipients at 2 dpf. Since these zebrafish have not developed a thymus at this stage of embryogenesis (Langenau and Zon, 2005), recipients do not reject the donor ganglioneuroma cells. After transplantation, embryos were given 24 h to recover, and then mTOR inhibitors or vehicle control (DMSO) were added to the fish water from 3 to 7 dpf (Fig. 5 A). In this assay, DMSO-treated cells showed similar mCherry signal at 7 dpf that they exhibited at 3 dpf, indicating that the cells did not die or grow appreciably in the pericardial environment over this 4-d period (Fig. 5, B and C). We tested both the mTOR kinase inhibitors, sirolimus and INK128, at their maximum tolerated dosages and found that these compounds each reduced the mCherry fluorescence intensity of the tumor mass by ∼50% at 7 dpf compared with 3 dpf, while DMSO-treated ganglioneuroma transplanted fish showed no change (Fig. 5, B and C). We also tested MK-2206, which is an allosteric inhibitor of AKT that suppresses AKT phosphorylation and activation. Since myr-Akt2 constitutively targets mAkt2 to the cell membrane and circumvents MK-2206's mode of action (Sefton et al., 2013), this compound acts as a negative control. Thus, this compound does not show activity in our myr-Akt2–expressing zebrafish ganglioneuroma cells (Fig. 5, B and C) but might exhibit activity in human ganglioneuroma, in which as-yet-unidentified upstream signals lead to the activation of endogenous AKT. Western blot analysis of primary zebrafish ganglioneuroma cells in vitro showed marked inhibition of phosphorylation of S6 ribosomal protein after treatment with

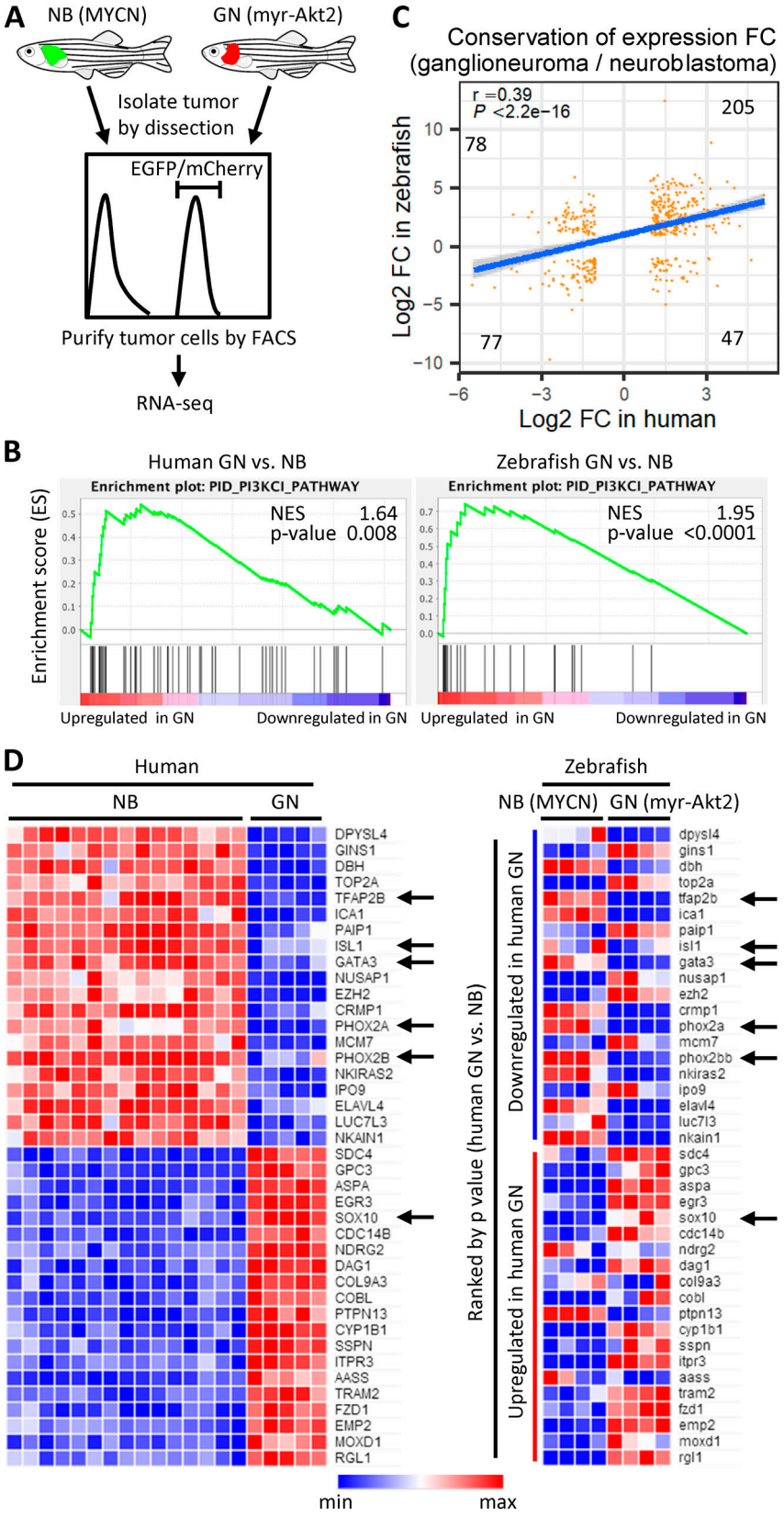

Figure 4. **Whole-transcriptome analysis of ganglioneuroma and neuroblastoma between human and zebrafish. (A)** Scheme of zebrafish RNA-seq. Zebrafish neuroblastoma (NB) and ganglioneuroma (GN) cells were isolated and sorted by FACS and subjected to RNA-seq. **(B)** CRC to determine enrichment of a gene signature for the PI3K pathway in both human and zebrafish ganglioneuroma versus neuroblastoma samples. Genes are ranked by score and plotted along the x axis as vertical black bars. NES, normalized enrichment score. **(C)** Highly correlated fold change (log_2 of ganglioneuroma/neuroblastoma) between human and zebrafish (Pearson's r = 0.39, P < 2.2e-16) in gene expression of 407 Biomart one-to-one orthologues with absolute log_2-fold-change >1. The linear regression line (blue) and 95% CI (surrounding shaded area) were plotted. Gene numbers within each group were indicated. **(D)** Heatmaps of top 20 down- or up-regulated genes (ranked by P value for human) in human and zebrafish. Arrows indicate key transcription factors in neuroblastoma and ganglioneuroma. Zebrafish RNA-seq was performed in quadruplicate for each condition.

sirolimus and more modest inhibition after treatment with INK128 (Fig. 5 D). By contrast, phosphorylated EIF4EBP1 was much more strongly inhibited by the mTOR kinase inhibitor INK128 (Fig. 5 D). Both DMSO and MK-2206 had no effects on phosphorylation of these substrates of mTOR (Fig. 5 D). Cellular DNA content analysis with DAPI staining showed a significant increase of cells in the sub-G1 area, representing increased apoptotic cells, in sirolimus- or INK128-treated primary zebrafish

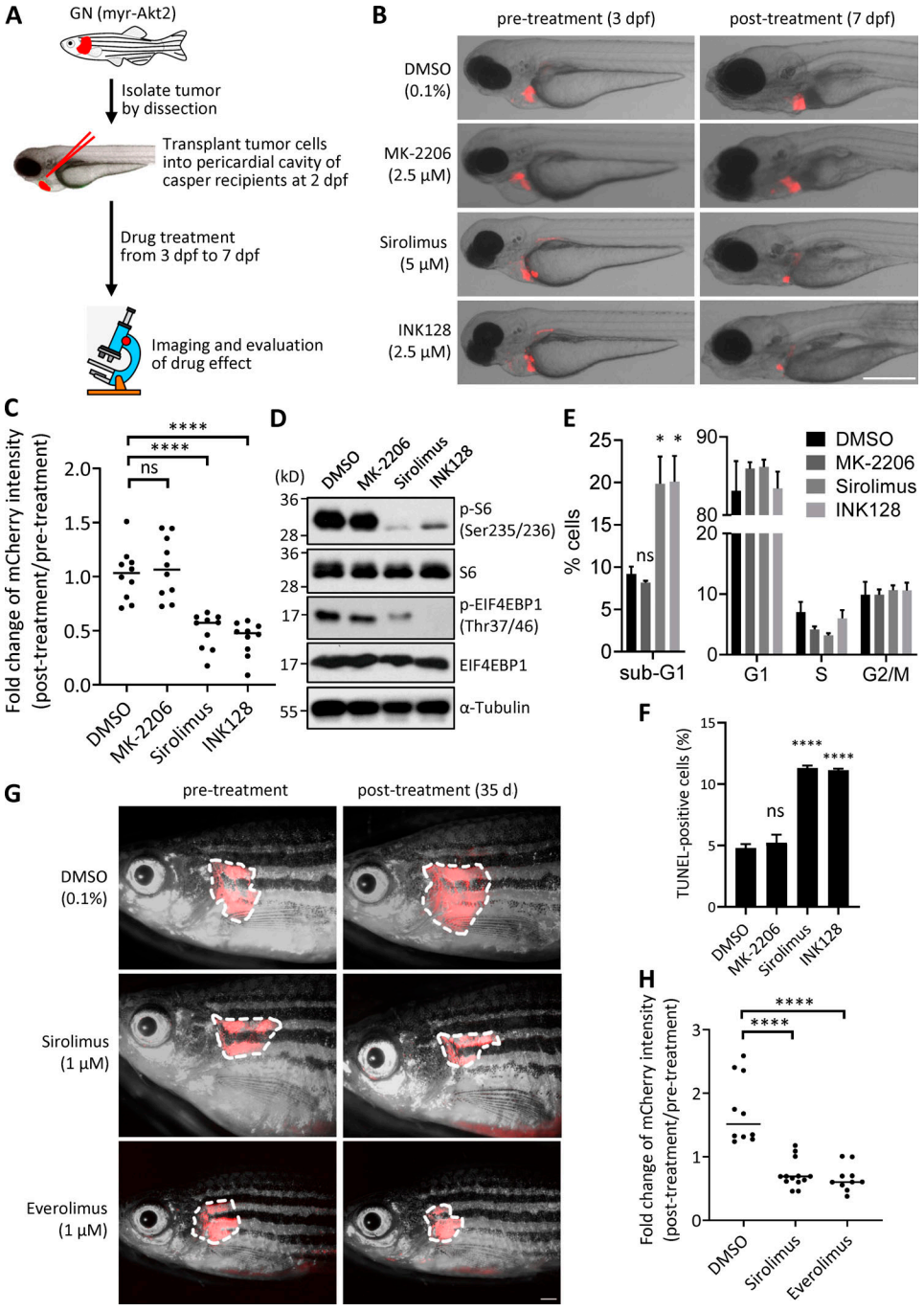

Figure 5. **mTOR inhibitors reduce tumor burden in zebrafish with ganglioneuroma. (A)** Experimental workflow of the embryonic transplantation assay. Zebrafish primary ganglioneuroma cells were isolated from myr-Akt2 tumor-bearing fish and 100–120 tumor cells were transplanted into the pericardial cavity of casper recipients at 2 dpf. Embryos were treated with compound from 3 dpf to 7 dpf. **(B)** Representative images of casper recipients pre- and posttreated with different compound as indicated. Scale bar, 500 μm. **(C)** Fold change of mCherry fluorescence intensity of the tumor cells transplanted into the casper recipients under different compound treatment. Each symbol represents the value for an individual embryo. Horizontal bars indicate medians that were compared with two-tailed Wilcoxon rank-sum test. Medians for MK-2206, sirolimus, and INK128 were compared with DMSO. ns, not significant; ****, $P < 0.0001$. **(D)** Western blotting of phosphorylated S6 ribosomal protein (p-S6; Ser235/236), S6, phosphorylated EIF4EBP1 (p-EIF4EBP1; Thr37/46), and EIF4EBP1 using the zebrafish primary ganglioneuroma cells treated with different compound for 18 h. α-Tubulin was used as a loading control. The positions of molecular weight markers are indicated. Data are representative of three independent experiments. **(E and F)** Zebrafish primary ganglioneuroma cells were treated with the indicated compound for 48 h. The percentages of cells in sub-G1 area and live cell events in G1, S, and G2/M phase of the cell cycle were analyzed with DAPI staining followed by flow cytometry (E). Apoptotic cells were determined by flow cytometry to measure the percentage of FITC-positive cells after TUNEL staining (F). Values are means ± SEM of three independent experiments. Means for MK-2206, sirolimus, and INK128 were compared with DMSO by two-tailed, unpaired *t* test. ns, not significant; *, $P < 0.05$; ****, $P < 0.0001$. **(G)** Representative images of adult ganglioneuroma-bearing fish before and after treatment of 8 h/d for 35 d with the indicated compound. Scale bar, 1 mm. **(H)** Fold change of mCherry fluorescence intensity of the tumor mass after treatment with each compound. Each symbol represents the value for an individual fish. Horizontal bars indicate medians that were compared with two-tailed Wilcoxon rank-sum test. ****, $P < 0.0001$.

ganglioneuroma cells when compared with MK-2206– or DMSO-treated cells (Fig. 5 E and Fig. S3 K). The percentages of cells in G1, S, and G2/M phase were not significantly altered by these drugs (Fig. 5 E and Fig. S3 K). A TUNEL assay with the same cells showed increased levels of TUNEL-positive cells in sirolimus- or INK128-treated zebrafish ganglioneuroma cells (Fig. 5 F and Fig. S3 L), further confirming the increased levels of apoptosis caused by treatment with these drugs. To test the efficacy of sirolimus and everolimus for shrinking the size of primary tumors in adult fish, we directly treated ganglioneuroma-bearing adult fish with DMSO, sirolimus (1 µM), or everolimus (1 µM) dissolved in the fish water for 8 h/d for a total of 35 d. Both sirolimus and everolimus effectively reduced the tumor burden by ∼30–40% after treatment, while the DMSO-treated group showed an ∼1.5-fold gain in tumor burden over this time period (Fig. 5, G and H). Thus, our results in the zebrafish model of ganglioneuroma indicate that sirolimus and everolimus effectively target ganglioneuroma cells in vivo, which we believe is significant because sirolimus and everolimus are well tolerated and already in clinical use in pediatrics for a variety of diseases.

In this study, we made the surprising discovery that AKT and its downstream mTOR–S6 pathway are activated, as detected by IHC with phospho-specific antibodies, much more frequently in the low-grade neuronal tumor ganglioneuroma than in neuroblastoma, its malignant high-grade counterpart within the PSNS (Fig. 1). We modeled this in vivo using a zebrafish engineered to express constitutively activated AKT in the PSNS. We found that fish overexpressing this oncogene developed low-grade ganglioneuroma with 40–50% penetrance during the first 29 wk of life (Fig. 2). These fish did not develop neuroblastoma, despite the fact that the same promoter-driven other oncogenes such as MYCN or c-MYC induces high-grade neuroblastoma in this model (Tao et al., 2017; Zimmerman et al., 2018; Zhu et al., 2012). Our zebrafish transgenic model overexpressing activated AKT in developing PSNS cells appears to be quite faithful to the human disease, which also exhibits activation of AKT. It will be important in future studies to analyze the underlying mechanisms and the effects of AKT and mTOR inhibitors on primary human ganglioneuroma cells, if they can be grown in short-term culture or as patient-derived xenograft models. Unfortunately, under current state-of-the-art conditions, human ganglioneuroma cells have not successfully engrafted in immune-deprived mice. Conditions that support short- and long-term culture of human primary ganglioneuroma cells also have not yet been identified. Presumably, these difficulties arise because human ganglioneuroma is a nonmetastatic, primarily differentiated tumor containing mature gangliocytes. Taken together, our studies in primary patient samples and zebrafish implicate activated AKT as a previously unappreciated driver of childhood ganglioneuroma. Ganglioneuromas that develop in activated AKT-overexpressing zebrafish are faithful to human ganglioneuromas by histological and gene expression analysis. Using this model, we implicate clinically available inhibitors of the mTOR kinase, which are approved by the Food and Drug Administration for use in pediatrics, as agents that reduce ganglioneuroma tumor burden in this disease.

The role of activated AKT in human neoplasia appears to be context dependent. Activation of the AKT pathway has been found in a number of malignant tumor types, including breast cancer, colorectal cancer, and squamous cell lung carcinoma, and has been shown to regulate multiple cellular processes in these types of cancer, including cell survival, proliferation, and apoptosis (Cheng et al., 2005; Engelman, 2009; Vanhaesebroeck et al., 2012). The role of AKT in neural crest–derived malignancies, however, appears to be quite different (Eleveld et al., 2015). AKT activity is broadly required throughout the development of neural crest for processes that include cell migration, differentiation, and maturation (Sittewelle and Monsoro-Burq, 2018). Ganglioneuroma and neuroblastoma both arise in children from neural crest–derived progenitor cells, but are distinct at many levels (Shimada and Ambros, 2005). Ganglioneuroma is a low-grade tumor in which cells exhibit differentiation toward mature ganglion cells and grow slowly by extension of the tumor mass, with rare local or widespread metastatic dissemination. By contrast, neuroblastoma cells resemble undifferentiated neuronal progenitors and often spread locally through the lymphatic drainage and disseminate hematogenous to bone marrow, liver, skin, and bone.

Our RNA-seq analysis of gene expression in zebrafish neuronal tumors exhibited a striking concordance with published human gene expression microarray results for both ganglioneuroma and neuroblastoma (Fig. 4). For example, the adrenergic CRC of human neuroblastoma recently identified by our group and other groups as a feed-forward autoregulatory loop composed of master transcription factors driven by super-enhancers and expressed at high levels was also expressed at high levels in zebrafish neuroblastomas driven by MYCN. These up-regulated master transcription factors in human and zebrafish neuroblastomas include *TFAP2B*, *ISL1*, *GATA3*, *PHOX2A*, and *PHOX2B* (Fig. 4), and high levels of expression are required to establish the malignant cell state in this subset of neuroblastoma (Boeva et al., 2017; Durbin et al., 2018; van Groningen et al., 2017). These transcription factors were not highly expressed by human and zebrafish ganglioneuromas overexpressing activated AKT, emphasizing the very different cell state of these low-grade tumors. By contrast, the expression of *SOX10*, a master transcription factor expressed by mature, differentiated ganglion cells and Schwann cells (Delfino-Machín et al., 2017), was remarkably up-regulated in human and zebrafish ganglioneuromas. Up-regulation of *SOX10* suggests that this transcription factor may play a role in regulating the differentiation of neuronal progenitor cells. Indeed, activated Akt is required for neural crest differentiation by regulation of Sox10 activity in zebrafish (Ciarlo et al., 2017). These examples serve to demonstrate the close similarity between human and zebrafish ganglioneuromas and emphasize the differences in gene expression as well as clinical behavior of these low-grade tumors compared with neuroblastoma.

The tuberous sclerosis complex (TSC) represents a well-studied human syndrome caused by gene mutations in *TSC1* and *TSC2*, with hyperactivation of the mTOR pathway. The TSC1–TSC2 protein complex is a tumor suppressor complex with inhibitory effects on the mTOR signaling cascade (Jeong and

Wong, 2016; Rosset et al., 2017). Patients with the clinical syndrome of tuberous sclerosis develop mature neuronal tumors called subependymal giant cell astrocytomas, which are characterized by ectopic activation of mTOR and are highly responsive to clinical use of mTOR inhibitors (Jeong and Wong, 2016). As low-grade neuronal tumors, these subependymal giant cell astrocytomas share many similarities with ganglioneuromas, including their propensity to exhibit expansive growth with rare regional or widespread dissemination. Intriguingly, mTOR inhibitors (sirolimus or everolimus) have been used to treat children with TSC, and these compounds are well tolerated by pediatric patients (Jeong and Wong, 2016; Krueger et al., 2018). Currently, patients with ganglioneuroma are treated by surgery alone, but this approach can be fraught with postoperative morbidities, including bowel dysfunction, chronic neuropathy, and vascular insufficiency, among others (Table S3; Decarolis et al., 2016; Sánchez-Galán et al., 2014). Our preclinical study suggests that sirolimus or other rapalogs would also be active for the presurgical treatment of children with ganglioneuroma, providing a means to reduce the size and extent of these tumors so that they can be more safely removed at the time of definitive surgical resection.

Our findings raise several important questions aside from the potential clinical impact of mTOR-targeting drugs on clinical management of ganglioneuroma patients, particularly those that are deemed surgically unresectable. Future studies are needed to define the upstream drivers of AKT Ser473 phosphorylation that induce ganglioneuroma. The primary pathways leading to AKT activation are often initiated by receptor tyrosine kinases or G-protein–coupled receptors leading to membrane recruitment and activation of one or more isoforms of PI3K, which in turn recruit and activate mTORC2, leading to AKT activation mediated by phosphorylation on Ser473 (Manning and Toker, 2017; Saxton and Sabatini, 2017). In Table S3, we list the inherited abnormalities in our series of children with ganglioneuroma. The most relevant is juvenile polyposis syndrome, such as that documented in patient 9, which may develop in the setting of *PTEN* and *BMPR1A* mutations (Busoni et al., 2019; Guaraldi et al., 2017). PTEN inactivation results in a loss of inhibition of AKT and, therefore, constitutive activation (Manning and Toker, 2017), which may provide insight into the etiology of ganglioneuroma in patients with this syndrome. Somatically acquired mutations or epigenetic alterations affecting the expression levels of proteins in the PI3K–AKT–mTOR pathway may be responsible for initiating ganglioneuroma in individual patients. In the future, whole-genome sequencing of matched tumor and normal genomic DNA will be needed to identify lesions that contribute to aberrant AKT signaling in ganglioneuroma. Although uncommon, familial cases of ganglioneuroma have been reported (Leavitt et al., 2000), and these provide a unique setting to identify causative mutations by whole-genome sequencing of affected compared with unaffected family members.

Materials and methods

Patient samples and IHC analysis

Human primary ganglioneuroma and poorly differentiated neuroblastoma samples were obtained from the archives of the Department of Pathology, Boston Children's Hospital (Table S1). Available samples with sufficient quality for IHC were identified from patients with ganglioneuroma, ganglioneuroblastoma, or neuroblastoma. Power calculations were performed using a two-sided Mantel-Haenszel test with $\alpha = 0.05$ to give a conservative estimate of the power provided by a Fisher's exact test. A sample size of $n = 12$ patients in each group would provide 80% power to detect a 54% difference in the proportion of patients positive for phosphorylated AKT for ganglioneuroma (89%) versus neuroblastoma (35%). H&E staining and IHC with primary antibodies against phosphorylated AKT (Ser473; 1:100, #4060; Cell Signaling Technology; recognizes p-AKT1 [Ser473], p-AKT2 [Ser474], and p-AKT3 [Ser472]); pan-AKT (1:200, #4691; Cell Signaling Technology; recognizes each of the AKT1, AKT2, and AKT3 isoforms), phospho-mTOR (Ser2448; 1:100, #2976; Cell Signaling Technology), mTOR (1:100, #2983; Cell Signaling Technology), phospho-S6 ribosomal protein (Ser235/236; 1:400, #4858; Cell Signaling Technology), and S6 ribosomal protein (1:100, #2317; Cell Signaling Technology) were performed at the DF/HCC Research Pathology Core. All IHC was performed using the Leica Bond III automated staining platform with the Leica Biosystems Refine Detection Kit with citrate antigen retrieval. Immunohistochemical staining was visually inspected by two independent observers, blinded to each other's analysis and any sample identifying information or diagnosis, and quantified by distribution of the stain in viable tumor cells. Scoring of sections was performed independently by each observer. Sections with <10% of viable tumor cells staining positively were considered negative (score of 0), and those with >25% of viable tumor cells staining positively were considered positive (score of 1). In our evaluation, no sections were identified with staining in an intermediate fashion (i.e., between 10 and 25% of viable tumor cells staining positively). Statistical comparisons of two groups were performed by two-sided Fisher's exact test (binary endpoint) or two-tailed Wilcoxon rank-sum test (continuous endpoint). Ganglioneuroma and neuroblastoma specimens were removed at surgery at Boston Children's Hospital. Patients and their parents or guardians provided informed consent that after all clinically relevant evaluations were performed, the remaining surgical specimens could be used for deidentified research purposes. The studies reported here, including the analysis of clinical features of the patients, were performed with the approval of the Dana-Farber Cancer Institute Institutional Review Board (DFCI protocol 19–150). All results are reported using arbitrary sample ID numbers without linked identifiers.

Fish lines and maintenance

AB background zebrafish were raised and maintained by standard procedures. All zebrafish studies and maintenance were done in accordance with Dana-Farber Cancer Institute institutional animal care and use committee (IACUC)–approved protocol #02-107.

Zebrafish lines *Tg(dβh:EGFP)*, *Tg(dβh:mCherry)*, and *Tg(dβh:EGFP-MYCN)* (Zhu et al., 2012; Zhu et al., 2017) were described previously and are designated EGFP, mCherry, and MYCN in the text, respectively. To generate zebrafish transgenic line *Tg(dβh:mCherry;dβh:myr-Akt2)*, a constitutively active *myr-Akt2* (Tan

et al., 2008) was subcloned under the *dβh* promoter (Zhu et al., 2012) using the primers 5′-CGGACCGGTACCATGGGGAGCAGC AAGAGCAAGCCC-3′ and 5′-CCGTTAATTAATCACTCTCGGATG CTGGCTGAGTA-3′. DNA constructs *dβh:mCherry* and *dβh:myr-Akt2* were linearized by I-SceI, followed by injection into zebrafish embryos at the one-cell stage using a coinjection strategy (Langenau et al., 2008). Mosaic F0 transgenic fish with germline integration were identified, and two independent stable *Tg(dβh:mCherry;dβh:myr-Akt2)* transgenic lines (myr-Akt2#1 and #2) were established from the F1 generation. The primer pair *mAkt2*_Fw665: 5′-ATGACCGCCTATGCTTTGTGA-3′ and *mAkt2*_Rv991: 5′-CTGCTC GCCCATAGTCATTGTC-3′ was used to genotype myr-Akt2#1 and #2 lines using the genomic DNA extracted from fin clips as template.

Tumor watch

Transgenic fish were observed biweekly for evidence of EGFP or mCherry fluorescent tumors starting at 7 wpf. Fish with tumors were separated, genotyped, and sacrificed after anesthesia and characterized by histopathological H&E staining and molecular analysis. Zebrafish ganglioneuromas and neuroblastomas were diagnosed based on their distinctive histopathologic features using H&E-stained sections. Zebrafish ganglioneuromas were composed of differentiated, large, mature ganglion cells that had similar cytological features as the paravertebral mature ganglion cells present nearby in the same zebrafish. The nuclear/cytoplasmic ratio was low, and round large nuclei with open chromatin were centrally located and had prominent single nucleoli. An eosinophilic, uniformly abundant cytoplasm was present in all ganglioneuroma cells (see Fig. 2 F). In contrast, zebrafish neuroblastomas were composed of undifferentiated, small, round neuroblasts with a high nuclear/cytoplasmic ratio, hyperchromatic nuclei, inconspicuous nucleoli, and scant cytoplasm (see Fig. 2 I). The cumulative frequency of tumor development was analyzed by the Kaplan–Meier method, and subgroups were compared with a two-sided log-rank test.

Embryonic transplantation assay

Zebrafish primary ganglioneuroma cells were isolated from myr-Akt2 tumor-bearing fish by dissection after tricaine overdose treatment according to IACUC-approved protocol. The tumor tissue was manually disrupted with a blade in a suspension solution (0.9× PBS + 5% FBS) and filtered through a 20-µm cell strainer (#NC9699018; Thermo Fisher Scientific). The tumor cells were then centrifuged and resuspended in the suspension solution at a density of 1.0–1.2 × 10^8 cells/ml. 1 nl of the tumor cells (100–120 cells) was transplanted into the pericardial cavity of casper recipients at 2 dpf. The transplanted embryos were given 24 h to recover. At 3 dpf, the embryos with successful transplants were collected, imaged, and subjected to compound treatment in 96-well plates. After compound treatment for 4 d, the embryos were imaged again, and tumor burden was calculated as the intensity of the mCherry fluorescence.

EdU pulse labeling, cryosectioning, paraffin sectioning, and immunostaining

For EdU pulse labeling experiments in zebrafish, EdU from the Click-iT Alexa Fluor 647 Imaging Kit (#C10340; Life Technologies) was diluted to 2.5 mg/ml for retro-orbital injection. Each euthanized fish examined at 5 wpf was injected with 1 µl EdU solution. Fish were fixed 2 h after injection for cryosectioning, and EdU detection was performed according to the manufacturer's protocol.

Zebrafish cryosectioning and immunofluorescence staining were performed as previously described (Tao et al., 2017). Fish at indicated stage were fixed in 4% paraformaldehyde at 4°C overnight, followed by washing with PBS three times. The samples were embedded in 1.5% agarose melted in 30% sucrose PBS solution and equilibrated in 30% sucrose PBS solution overnight at 4°C. Sagittal sections were cut serially at a 14-µm thickness and then collected on CLIP CRNR EXCELL slides (#22-037-247; Thermo Fisher Scientific). For immunofluorescence staining, slides were incubated with a primary antibody at 4°C overnight, washed with PBS/0.1% Tween 20 (PBST), and then incubated with a secondary antibody for 2 h at room temperature. An antibody against EGFP (#A11120; Life Technologies) was used as a primary antibody. Secondary antibodies were conjugated with Alexa Fluor 488, 568, and 647 (Life Technologies). DAPI (#S36973; Life Technologies) was used for nuclear staining. Fluorescent images were taken by a Leica SP5X scanning confocal microscope at the Confocal and Light Microscopy core facility at Dana-Farber Cancer Institute.

Zebrafish paraffin sectioning, H&E staining, and IHC with primary antibodies against phospho-AKT (Ser473, #4060; Cell Signaling Technology), pan-AKT (#4691; Cell Signaling Technology), TH (#P40101; Pel-Freez), HuC (#A-21271; Life Technologies), phospho-mTOR (Ser2448; Cell Signaling Technology #2976), phospho-S6 ribosomal protein (Ser235/236, #4858; Cell Signaling Technology), phospho-EIF4EBP1 (Thr37/46, #2855; Cell Signaling Technology), and Synaptophysin (#MAB5258; Millipore) were performed at the DF/HCC (Dana-Farber/Harvard Cancer Center) Research Pathology Core.

Zebrafish ganglioneuroma cell cycle and apoptosis analysis

Zebrafish primary ganglioneuroma cells were isolated from myr-Akt2 tumor-bearing fish by dissection after tricaine overdose treatment according to IACUC-approved protocol. The tumor tissue was manually disrupted with a blade in a suspension solution (0.9× PBS + 5% FBS) and filtered through a 20-µm cell strainer (#NC9699018; Thermo Fisher Scientific). The tumor cells were then centrifuged, resuspended in Leibovitz's L-15 medium (#31415029; GIBCO; Choorapoikayil et al., 2013) and seeded in a 6-well plate at a density of 1 × 10^6 cells per well. Cells were treated with vehicle (DMSO) or compound for 48 h. Cells were collected and either stained with DAPI for cell cycle analysis or subjected to a TUNEL assay (In situ Cell Death Detection Kit, Fluorescein, #11684795910; Roche) for apoptosis analysis. Cell number was recorded by a BD LSRFortessa flow cytometer. Data were analyzed using FlowJo v10 (BD Biosciences).

Compound treatment of adult ganglioneuroma-bearing fish

Zebrafish with primary ganglioneuroma at 8–12 mo old were treated with vehicle (DMSO), sirolimus (1 µM), or everolimus (1 µM) dissolved in 300 ml fish water for 8 h/d (9 a.m. to 5 p.m.). At 5 p.m. each day, the fish were transferred to 300 ml fresh fish

water containing 20 ml concentrated live rotifers, which were the nutritional source for the zebrafish during treatment. This treatment protocol was continued for a total of 35 d. Images were taken before and after treatment, and tumor burden was calculated as the intensity of the mCherry fluorescence.

Quantification and statistical analyses

To analyze the hyperplasia of the sympathoadrenal cells before tumor onset, all sections from each individual fish were scanned by confocal z-stack. A single representative section containing the largest number of sympathoadrenal cells in the IRG was selected and quantified for each individual fish. Data were compared with a two-tailed Wilcoxon rank-sum test.

To analyze the proliferative capacity of the sympathoadrenal cells before tumor onset, all sections from each individual fish were scanned by confocal z-stack. A single representative section containing the largest percentage of EdU^+ sympathoadrenal cells to the total number of sympathoadrenal cells in the IRG was selected and quantified for each individual fish. The data were analyzed by two-tailed Wilcoxon rank-sum test.

RNA-seq and data analysis

Zebrafish tumor cells of 6-mo-old fish were dissected and sorted by fluorescence. RNA samples were prepared and subjected to library preparation for Illumina NextSeq 500 Next-Generation Sequencing at the DFCI Molecular Biology Core Facilities. After acquiring the raw fastq format paired-end RNA-seq reads, we inspected the sequencing quality using fastqc v0.11.5 (https://www.bioinformatics.babraham.ac.uk/projects/fastqc/) and removed standard Illumina adapters from the 3′ end using Trim Galore v0.4.4 (https://www.bioinformatics.babraham.ac.uk/projects/trim_galore/). The processed reads were then aligned to the GRCz10 version of the zebrafish reference genome using Tophat v2.1.1 (Trapnell et al., 2009). The gene transfer format UCSC gene models, obtained from the iGenomes website (https://support.illumina.com/sequencing/sequencing_software/igenome.html), were provided as an annotation reference (-G option of Tophat). After the alignment, the BAM format files were sorted by reads name using Samtools v1.5 (Li et al., 2009), and the reads mapped to each gene were counted using HTSeq-count v0.6.1 (Anders et al., 2015). edgeR library (Robinson et al., 2010) was applied to normalize read counts across samples and identify genes that are differentially expressed between conditions in R. Zebrafish RNA-seq data in this study are available from the GEO under accession number GSE135682.

Human ganglioneuroma and neuroblastoma microarray data analysis

Human ganglioneuroma and neuroblastoma microarray data were obtained from the GEO under accession number GSE7529. The raw intensity data were reprocessed using the affy library (Gautier et al., 2004) in a way that is similar to the original procedures (Albino et al., 2008), i.e., no background correction, vsn method normalization, only perfectly matched probes accepted, and expression measured with the median polish approach. The limma library was applied to identify the differentially expressed genes between these two groups.

GSEA

Normalized expression values for individual samples of zebrafish RNA-seq (by edgeR) or human microarray (by limma) data were used for GSEA. Genes from whole transcriptomic data were ranked based on the $\log_2$-fold-change in ganglioneuroma versus neuroblastoma. The preranked option of GSEA (Subramanian et al., 2005) was run with 2500 permutations for statistical evaluation. GSEA was performed with signatures from version 6.0 of the molecular signature database (MolSigDB; http://www.broadinstitute.org/gsea/msigdb/index.jsp).

Protein extraction and Western blot analysis

Protein was extracted from zebrafish primary ganglioneuroma cells using RIPA buffer after compound treatment for 18 h. Western blotting was performed as described previously (Tao et al., 2013). Protein samples were separated by a 10% polyacrylamide gel and transferred to a polyvinylidene fluoride membrane (#PI88518; Thermo Fisher Scientific). The membrane was blocked in PBST containing 5% nonfat milk for 1 h at room temperature, incubated with a primary antibody for 2 h diluted in blocking buffer. After washing three times in PBST, the membrane was incubated with a secondary antibody for 1 h diluted in blocking buffer and washed three times again in PBST. The results were visualized on autoradiography films with SuperSignal West Pico Chemiluminescent Substrate (#PI34080; Pierce) or SuperSignal West Dura Extended Duration Substrate (#34075; Pierce). Antibodies against phospho-S6 ribosomal protein (Ser235/236, #2211; Cell Signaling Technology), S6 ribosomal protein (#2317; Cell Signaling Technology), phospho-EIF4EBP1 (Thr37/46, #2855; Cell Signaling Technology), EIF4EBP1 (#9644; Cell Signaling Technology), and α-Tubulin (#T6074; Sigma) were used as primary antibodies.

Online supplemental material

Fig. S1 shows immunohistochemical evaluation of mTOR and S6 protein activation in human primary ganglioneuromas and poorly differentiated neuroblastomas. Fig. S2 shows immunohistochemical analyses of normal IRG and neuroblastic tumors in myr-Akt2 and MYCN transgenic fish. Fig. S3 shows cellular phenotype of the sympathoadrenal lineage in the IRG of myr-Akt2 fish at 5 wpf and flow cytometry analysis of zebrafish primary ganglioneuroma cells treated with different compounds. Table S1 shows the demographic characteristics of patients included in this study. Table S2 shows the expression data of 4,321 orthologues in human and zebrafish ganglioneuroma and neuroblastoma. Table S3 shows the tumor characteristics of patients.

Acknowledgments

We thank Grace Thurston, Daniel Debiasi, Michael T. Coute, and Monica Alves for their excellent care of the zebrafish and Zachary T. Herbert of the Dana-Farber Molecular Biology Core Facility for genomics support. We thank Dana-Farber/Harvard Cancer Center in Boston, MA, for the use of the Specialized Histopathology Core, which provided histology and IHC service.

Dana-Farber/Harvard Cancer Center is supported in part by National Institutes of Health National Cancer Institute cancer

center support grant 5 P30 CA06516. This work was supported by a National Institutes of Health grant (R01-CA180692 to A.T. Look and J.M. Maris co-principal investigator grant). T. Tao was supported by the Pediatric Cancer Research Foundation, the Rally Foundation for Childhood Cancer Research, and Open Hands Overflowing Hearts. A.D. Durbin was supported by the Rally Foundation for Childhood Cancer Research, the CureSearch for Children's Cancer Foundation, and the American Society of Clinical Oncology. A.D. Durbin is a Damon Runyon-Sohn Pediatric Fellow (DRSG-24-18). A.D. Durbin and H. Shi are recipients of Alex's Lemonade Stand Foundation for Childhood Cancer Young Investigator awards.

Author contributions: T. Tao, H. Shi, A.D. Durbin, and A.T. Look were responsible for the concept and design; T. Tao and H. Shi performed the zebrafish and human experiments and analyzed the data; A.D. Durbin and W.B. London collected and performed the statistical analysis of the patients' demographic data; M. Wang, T. Tao, and B. Lemos performed the bioinformatics analysis; A.R. Perez-Atayde performed the pathology analysis; A. Gutierrez provided material support; and T. Tao, A.D. Durbin, and A.T. Look drafted and finalized the manuscript with input from all other authors.

Disclosures: T. Tao reported grants from Pediatric Cancer Research Foundation and grants from Rally Foundation for Childhood Cancer Research and the Open Hands Overflowing Hearts during the conduct of the study. H. Shi reported grants from Alex's Lemonade Stand Foundation during the conduct of the study. A.T. Look reported grants from National Institutes of Health during the conduct of the study. No other disclosures were reported.

Submitted: 3 October 2019
Revised: 1 April 2020
Accepted: 13 May 2020

References

Abdulkader, M.M., M.F. Dalesandro, S.K. Mendenhall, M.V. Shah, and J.M. Bonnin. 2016. Ciliochoroidal ganglioneuroma in neurofibromatosis type 1: Report of a case and review of the literature. *Neuropathology*. 36: 464–469. https://doi.org/10.1111/neup.12286

Albino, D., P. Scaruffi, S. Moretti, S. Coco, M. Truini, C. Di Cristofano, A. Cavazzana, S. Stigliani, S. Bonassi, and G.P. Tonini. 2008. Identification of low intratumoral gene expression heterogeneity in neuroblastic tumors by genome-wide expression analysis and game theory. *Cancer*. 113: 1412–1422. https://doi.org/10.1002/cncr.23720

Alexander, W.. 2011. Inhibiting the akt pathway in cancer treatment: three leading candidates. *P&T*. 36:225–227.

Alexander, N., K. Sullivan, F. Shaikh, and M.S. Irwin. 2018. Characteristics and management of ganglioneuroma and ganglioneuroblastoma-intermixed in children and adolescents. *Pediatr. Blood Cancer*. 65. e26964. https://doi.org/10.1002/pbc.26964

Anders, S., P.T. Pyl, and W. Huber. 2015. HTSeq--a Python framework to work with high-throughput sequencing data. *Bioinformatics*. 31:166–169. https://doi.org/10.1093/bioinformatics/btu638

Boeva, V., C. Louis-Brennetot, A. Peltier, S. Durand, C. Pierre-Eugène, V. Raynal, H.C. Etchevers, S. Thomas, A. Lermine, E. Daudigeos-Dubus, et al. 2017. Heterogeneity of neuroblastoma cell identity defined by transcriptional circuitries. *Nat. Genet*. 49:1408–1413. https://doi.org/10.1038/ng.3921

Busoni, V.B., M. Orsi, P.A. Lobos, D. D'Agostino, M. Wagener, P. De la Iglesia, and V.L. Fox. 2019. Successful Treatment of Juvenile Polyposis of Infancy With Sirolimus. *Pediatrics*. 144. e20182922. https://doi.org/10.1542/peds.2018-2922

Cheng, J.Q., C.W. Lindsley, G.Z. Cheng, H. Yang, and S.V. Nicosia. 2005. The Akt/PKB pathway: molecular target for cancer drug discovery. *Oncogene*. 24:7482–7492. https://doi.org/10.1038/sj.onc.1209088

Cheung, N.K., and M.A. Dyer. 2013. Neuroblastoma: developmental biology, cancer genomics and immunotherapy. *Nat. Rev. Cancer*. 13:397–411. https://doi.org/10.1038/nrc3526

Choorapoikayil, S., J. Overvoorde, and J. den Hertog. 2013. Deriving cell lines from zebrafish embryos and tumors. *Zebrafish*. 10:316–325. https://doi.org/10.1089/zeb.2013.0866

Ciarlo, C., C.K. Kaufman, B. Kinikoglu, J. Michael, S. Yang, C. D Amato, S. Blokzijl-Franke, J. den Hertog, T.M. Schlaeger, Y. Zhou, et al. 2017. A chemical screen in zebrafish embryonic cells establishes that Akt activation is required for neural crest development. *eLife*. 6. e29145. https://doi.org/10.7554/eLife.29145

Decarolis, B., T. Simon, B. Krug, I. Leuschner, C. Vokuhl, P. Kaatsch, D. von Schweinitz, T. Klingebiel, I. Mueller, L. Schweigerer, et al. 2016. Treatment and outcome of Ganglioneuroma and Ganglioneuroblastoma intermixed. *BMC Cancer*. 16:542. https://doi.org/10.1186/s12885-016-2513-9

Delfino-Machín, M., R. Madelaine, G. Busolin, M. Nikaido, S. Colanesi, K. Camargo-Sosa, E.W. Law, S. Toppo, P. Blader, N. Tiso, et al. 2017. Sox10 contributes to the balance of fate choice in dorsal root ganglion progenitors. *PLoS One*. 12. e0172947. https://doi.org/10.1371/journal.pone.0172947

Durbin, A.D., M.W. Zimmerman, N.V. Dharia, B.J. Abraham, A.B. Iniguez, N. Weichert-Leahey, S. He, J.M. Krill-Burger, D.E. Root, F. Vazquez, et al. 2018. Selective gene dependencies in MYCN-amplified neuroblastoma include the core transcriptional regulatory circuitry. *Nat. Genet*. 50: 1240–1246. https://doi.org/10.1038/s41588-018-0191-z

Eleveld, T.F., D.A. Oldridge, V. Bernard, J. Koster, L. Colmet Daage, S.J. Diskin, L. Schild, N.B. Bentahar, A. Bellini, M. Chicard, et al. 2015. Relapsed neuroblastomas show frequent RAS-MAPK pathway mutations. *Nat. Genet*. 47:864–871. https://doi.org/10.1038/ng.3333

Engelman, J.A.. 2009. Targeting PI3K signalling in cancer: opportunities, challenges and limitations. *Nat. Rev. Cancer*. 9:550–562. https://doi.org/10.1038/nrc2664

Gautier, L., L. Cope, B.M. Bolstad, and R.A. Irizarry. 2004. affy--analysis of Affymetrix GeneChip data at the probe level. *Bioinformatics*. 20:307–315. https://doi.org/10.1093/bioinformatics/btg405

Guaraldi, F., G. Di Nardo, L. Tarani, L. Bertelli, F.C. Susca, R. Bagnulo, and N. Resta. 2017. Association of autoimmune thyroiditis and celiac disease with Juvenile Polyposis due to 10q23.1q23.31 deletion: Potential role of PI3K/Akt pathway dysregulation. *Eur. J. Med. Genet*. 60:380–384. https://doi.org/10.1016/j.ejmg.2017.04.010

Huang, M., and W.A. Weiss. 2013. Neuroblastoma and MYCN. *Cold Spring Harb. Perspect. Med*. 3. a014415. https://doi.org/10.1101/cshperspect.a014415

Irie, H.Y., R.V. Pearline, D. Grueneberg, M. Hsia, P. Ravichandran, N. Kothari, S. Natesan, and J.S. Brugge. 2005. Distinct roles of Akt1 and Akt2 in regulating cell migration and epithelial-mesenchymal transition. *J. Cell Biol*. 171:1023–1034. https://doi.org/10.1083/jcb.200505087

Jeong, A., and M. Wong. 2016. mTOR Inhibitors in Children: Current Indications and Future Directions in Neurology. *Curr. Neurol. Neurosci. Rep*. 16:102. https://doi.org/10.1007/s11910-016-0708-8

Krueger, D.A., J.K. Capal, P. Curatolo, O. Devinsky, K. Ess, M. Tzadok, M.K. Koenig, V. Narayanan, F. Ramos, S. Jozwiak, et al; TSCure Research Group. 2018. Short-term safety of mTOR inhibitors in infants and very young children with tuberous sclerosis complex (TSC): Multicentre clinical experience. *Eur. J. Paediatr. Neurol*. 22:1066–1073. https://doi.org/10.1016/j.ejpn.2018.06.007

Langenau, D.M., and L.I. Zon. 2005. The zebrafish: a new model of T-cell and thymic development. *Nat. Rev. Immunol*. 5:307–317. https://doi.org/10.1038/nri1590

Langenau, D.M., M.D. Keefe, N.Y. Storer, C.A. Jette, A.C. Smith, C.J. Ceol, C. Bourque, A.T. Look, and L.I. Zon. 2008. Co-injection strategies to modify radiation sensitivity and tumor initiation in transgenic Zebrafish. *Oncogene*. 27:4242–4248. https://doi.org/10.1038/onc.2008.56

Leavitt, J.R., D.L. Harold, and R.B. Robinson. 2000. Adrenal ganglioneuroma: a familial case. *Urology*. 56:508. https://doi.org/10.1016/S0090-4295(00)00695-6

Li, H., B. Handsaker, A. Wysoker, T. Fennell, J. Ruan, N. Homer, G. Marth, G. Abecasis, and R. Durbin; 1000 Genome Project Data Processing Subgroup. 2009. The Sequence Alignment/Map format and SAMtools.

Bioinformatics. 25:2078–2079. https://doi.org/10.1093/bioinformatics/btp352

Lonergan, G.J., C.M. Schwab, E.S. Suarez, and C.L. Carlson. 2002. Neuroblastoma, ganglioneuroblastoma, and ganglioneuroma: radiologic-pathologic correlation. *Radiographics*. 22:911–934. https://doi.org/10.1148/radiographics.22.4.g02jl15911

Lora, M.S., S.G. Waguespack, J.F. Moley, and E.C. Walvoord. 2005. Adrenal ganglioneuromas in children with multiple endocrine neoplasia type 2: a report of two cases. *J. Clin. Endocrinol. Metab*. 90:4383–4387. https://doi.org/10.1210/jc.2004-2526

Maksoud, I., and L. Kassab. 2015. Rapid-onset obesity, hypoventilation, hypothalamic dysfunction, autonomic dysregulation syndrome. *Avicenna J. Med*. 5:89–94. https://doi.org/10.4103/2231-0770.160248

Manning, B.D., and A. Toker. 2017. AKT/PKB Signaling: Navigating the Network. *Cell*. 169:381–405. https://doi.org/10.1016/j.cell.2017.04.001

Matthay, K.K., J.M. Maris, G. Schleiermacher, A. Nakagawara, C.L. Mackall, L. Diller, and W.A. Weiss. 2016. Neuroblastoma. *Nat. Rev. Dis. Primers*. 2:16078. https://doi.org/10.1038/nrdp.2016.78

Puig, I., D. Champeval, P. De Santa Barbara, F. Jaubert, S. Lyonnet, and L. Larue. 2009. Deletion of Pten in the mouse enteric nervous system induces ganglioneuromatosis and mimics intestinal pseudoobstruction. *J. Clin. Invest*. 119:3586–3596. https://doi.org/10.1172/JCI39929

Retrosi, G., M. Bishay, E.M. Kiely, N.J. Sebire, J. Anderson, M. Elliott, D.P. Drake, P. Coppi, S. Eaton, and A. Pierro. 2011. Morbidity after ganglioneuroma excision: is surgery necessary? *Eur. J. Pediatr. Surg*. 21:33–37. https://doi.org/10.1055/s-0030-1263195

Robinson, M.D., D.J. McCarthy, and G.K. Smyth. 2010. edgeR: a Bioconductor package for differential expression analysis of digital gene expression data. *Bioinformatics*. 26:139–140. https://doi.org/10.1093/bioinformatics/btp616

Rosset, C., C.B.O. Netto, and P. Ashton-Prolla. 2017. TSC1 and TSC2 gene mutations and their implications for treatment in Tuberous Sclerosis Complex: a review. *Genet. Mol. Biol*. 40:69–79. https://doi.org/10.1590/1678-4685-gmb-2015-0321

Sánchez-Galán, A., S. Barrena, A. Vilanova-Sánchez, S.H. Martín, S. Lopez-Fernandez, P. García, M. Lopez-Santamaria, L. Martínez, and J.A. Tovar. 2014. Ganglioneuroma: to operate or not to operate. *Eur. J. Pediatr. Surg*. 24:25–30. https://doi.org/10.1055/s-0033-1358790

Saxton, R.A., and D.M. Sabatini. 2017. mTOR Signaling in Growth, Metabolism, and Disease. *Cell*. 168:960–976. https://doi.org/10.1016/j.cell.2017.02.004

Sefton, E.C., W. Qiang, V. Serna, T. Kurita, J.J. Wei, D. Chakravarti, and J.J. Kim. 2013. MK-2206, an AKT inhibitor, promotes caspase-independent cell death and inhibits leiomyoma growth. *Endocrinology*. 154:4046–4057. https://doi.org/10.1210/en.2013-1389

Shimada, H., and I.M. Ambros. 2005. Pathology of Peripheral Neuroblastic Tumors. *In* Neuroblastoma. N.V. Cheung, and S.L. Cohn, editors. Springer-Verlag, Berlin, Heidelberg. pp. 87–95. https://doi.org/10.1007/3-540-26616-X_8

Shimada, H., I.M. Ambros, L.P. Dehner, J. Hata, V.V. Joshi, and B. Roald. 1999a. Terminology and morphologic criteria of neuroblastic tumors: recommendations by the International Neuroblastoma Pathology Committee. *Cancer*. 86:349–363. https://doi.org/10.1002/(SICI)1097-0142(19990715)86:2<349::AID-CNCR20>3.0.CO;2-Y

Shimada, H., I.M. Ambros, L.P. Dehner, J. Hata, V.V. Joshi, B. Roald, D.O. Stram, R.B. Gerbing, J.N. Lukens, K.K. Matthay, and R.P. Castleberry. 1999b. The International Neuroblastoma Pathology Classification (the Shimada system). *Cancer*. 86:364–372. https://doi.org/10.1002/(SICI)1097-0142(19990715)86:2<364::AID-CNCR21>3.0.CO;2-7

Shohet, J., and J. Foster. 2017. Neuroblastoma. *BMJ*. 357:j1863. https://doi.org/10.1136/bmj.j1863

Sittewelle, M., and A.H. Monsoro-Burq. 2018. AKT signaling displays multifaceted functions in neural crest development. *Dev. Biol*. 444(Suppl 1):S144–S155. https://doi.org/10.1016/j.ydbio.2018.05.023

Subramanian, A., P. Tamayo, V.K. Mootha, S. Mukherjee, B.L. Ebert, M.A. Gillette, A. Paulovich, S.L. Pomeroy, T.R. Golub, E.S. Lander, et al. 2005. Gene set enrichment analysis: a knowledge-based approach for interpreting genome-wide expression profiles. *Proc. Natl. Acad. Sci. USA*. 102:15545–15550. https://doi.org/10.1073/pnas.0506580102

Sweetser, D.A., R.P. Kapur, G.J. Froelick, K.E. Kafer, and R.D. Palmiter. 1997. Oncogenesis and altered differentiation induced by activated Ras in neuroblasts of transgenic mice. *Oncogene*. 15:2783–2794. https://doi.org/10.1038/sj.onc.1201452

Sweetser, D.A., G.J. Froelick, A.M. Matsumoto, K.E. Kafer, B. Marck, R.D. Palmiter, and R.P. Kapur. 1999. Ganglioneuromas and renal anomalies are induced by activated RET(MEN2B) in transgenic mice. *Oncogene*. 18:877–886. https://doi.org/10.1038/sj.onc.1202376

Tan, Y., R.A. Timakhov, M. Rao, D.A. Altomare, J. Xu, Z. Liu, Q. Gao, S.C. Jhanwar, A. Di Cristofano, D.L. Wiest, et al. 2008. A novel recurrent chromosomal inversion implicates the homeobox gene Dlx5 in T-cell lymphomas from Lck-Akt2 transgenic mice. *Cancer Res*. 68:1296–1302. https://doi.org/10.1158/0008-5472.CAN-07-3218

Tao, T., H. Shi, Y. Guan, D. Huang, Y. Chen, D.P. Lane, J. Chen, and J. Peng. 2013. Def defines a conserved nucleolar pathway that leads p53 to proteasome-independent degradation. *Cell Res*. 23:620–634. https://doi.org/10.1038/cr.2013.16

Tao, T., S.B. Sondalle, H. Shi, S. Zhu, A.R. Perez-Atayde, J. Peng, S.J. Baserga, and A.T. Look. 2017. The pre-rRNA processing factor DEF is rate limiting for the pathogenesis of MYCN-driven neuroblastoma. *Oncogene*. 36:3852–3867. https://doi.org/10.1038/onc.2016.527

Trapnell, C., L. Pachter, and S.L. Salzberg. 2009. TopHat: discovering splice junctions with RNA-Seq. *Bioinformatics*. 25:1105–1111. https://doi.org/10.1093/bioinformatics/btp120

Trochet, D., F. Bourdeaut, I. Janoueix-Lerosey, A. Deville, L. de Pontual, G. Schleiermacher, C. Coze, N. Philip, T. Frébourg, A. Munnich, et al. 2004. Germline mutations of the paired-like homeobox 2B (PHOX2B) gene in neuroblastoma. *Am. J. Hum. Genet*. 74:761–764. https://doi.org/10.1086/383253

van Groningen, T., J. Koster, L.J. Valentijn, D.A. Zwijnenburg, N. Akogul, N.E. Hasselt, M. Broekmans, F. Haneveld, N.E. Nowakowska, J. Bras, et al. 2017. Neuroblastoma is composed of two super-enhancer-associated differentiation states. *Nat. Genet*. 49:1261–1266. https://doi.org/10.1038/ng.3899

Vanhaesebroeck, B., L. Stephens, and P. Hawkins. 2012. PI3K signalling: the path to discovery and understanding. *Nat. Rev. Mol. Cell Biol*. 13:195–203. https://doi.org/10.1038/nrm3290

Weiss, W.A., K. Aldape, G. Mohapatra, B.G. Feuerstein, and J.M. Bishop. 1997. Targeted expression of MYCN causes neuroblastoma in transgenic mice. *EMBO J*. 16:2985–2995. https://doi.org/10.1093/emboj/16.11.2985

Yamasaki, M., Y. Sato, T. Nomura, F. Sato, S. Uchino, and H. Mimata. 2017. Composite paraganglioma-ganglioneuroma concomitant with adrenal metastasis of medullary thyroid carcinoma in a patient with multiple endocrine neoplasia type 2B: A case report. *Asian J. Endosc. Surg*. 10:66–69. https://doi.org/10.1111/ases.12332

Zhu, S., J.S. Lee, F. Guo, J. Shin, A.R. Perez-Atayde, J.L. Kutok, S.J. Rodig, D.S. Neuberg, D. Helman, H. Feng, et al. 2012. Activated ALK collaborates with MYCN in neuroblastoma pathogenesis. *Cancer Cell*. 21:362–373. https://doi.org/10.1016/j.ccr.2012.02.010

Zhu, S., X. Zhang, N. Weichert-Leahey, Z. Dong, C. Zhang, G. Lopez, T. Tao, S. He, A.C. Wood, D. Oldridge, et al. 2017. LMO1 Synergizes with MYCN to Promote Neuroblastoma Initiation and Metastasis. *Cancer Cell*. 32:310–323.e5. https://doi.org/10.1016/j.ccell.2017.08.002

Zimmerman, M.W., Y. Liu, S. He, A.D. Durbin, B.J. Abraham, J. Easton, Y. Shao, B. Xu, S. Zhu, X. Zhang, et al. 2018. *MYC* Drives a Subset of High-Risk Pediatric Neuroblastomas and Is Activated through Mechanisms Including Enhancer Hijacking and Focal Enhancer Amplification. *Cancer Discov*. 8:320–335. https://doi.org/10.1158/2159-8290.CD-17-0993

Supplemental material

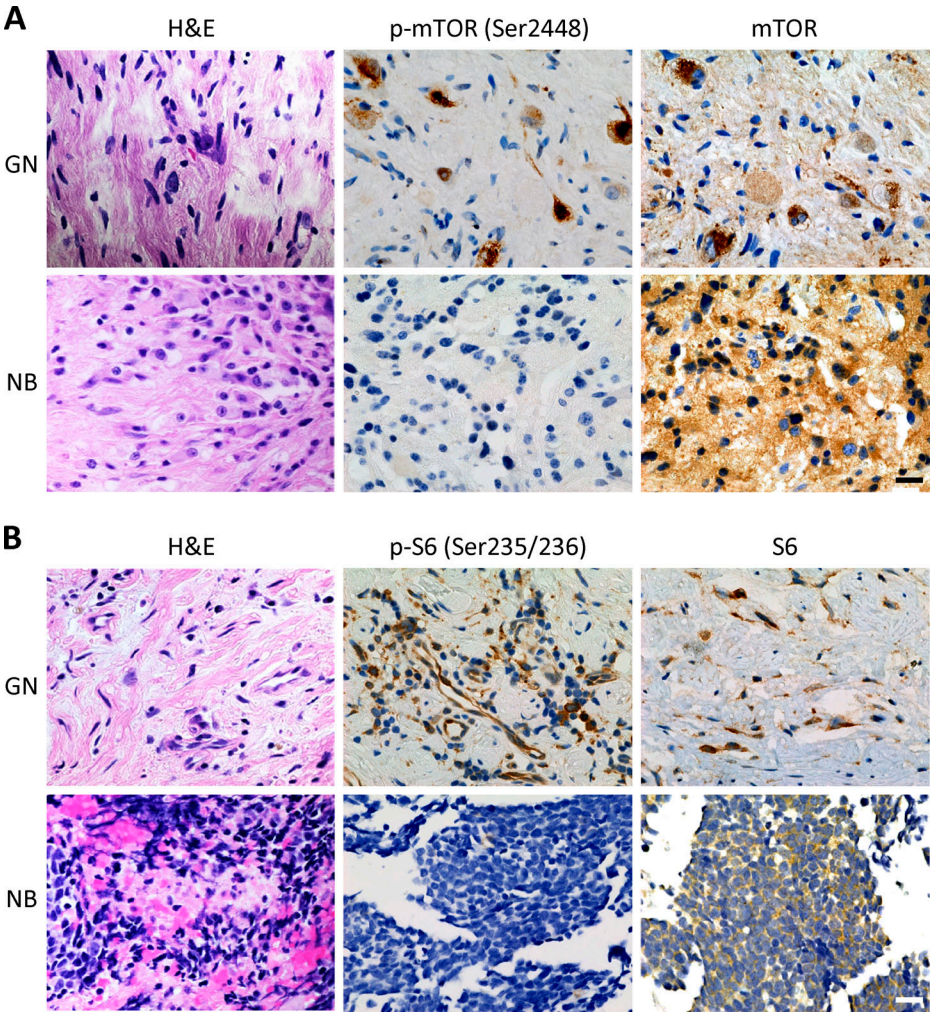

Figure S1. **Immunohistochemical evaluation of mTOR and S6 proteins phosphorylation in human primary ganglioneuromas and poorly differentiated neuroblastomas. (A)** H&E staining and IHC with phosphorylated mTOR (p-mTOR; Ser2448) and mTOR for a representative human primary ganglioneuroma (GN) and poorly differentiated neuroblastoma (NB). **(B)** H&E staining and IHC with phosphorylated S6 ribosomal protein (p-S6; Ser235/236) and S6 for a representative GN and NB. All scale bars represent 20 µm. Protein expression is indicated by brown staining.

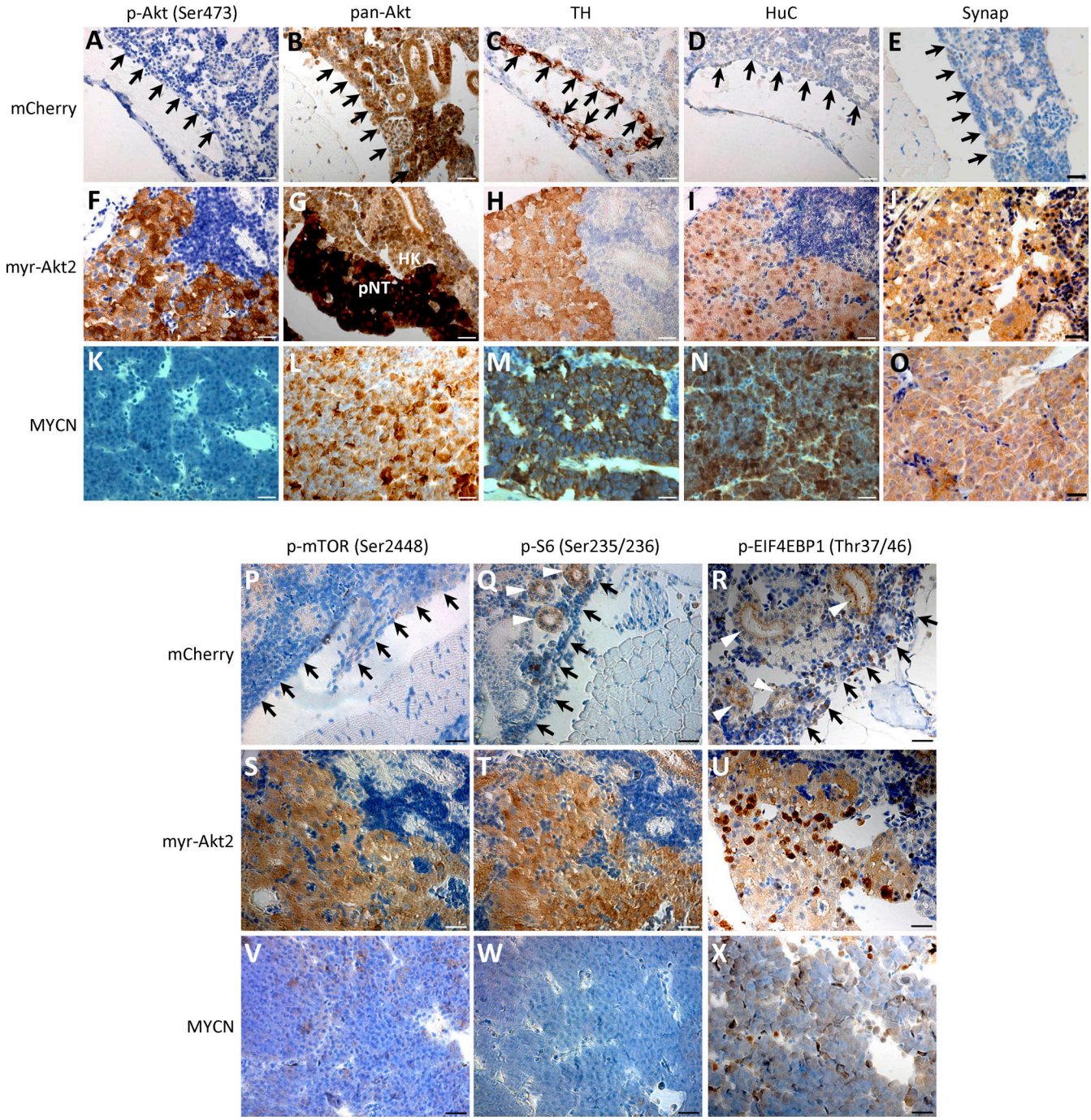

Figure S2. **Immunohistochemical analyses of normal IRG and neuroblastic tumors in myr-Akt2 and MYCN transgenic fish. (A–O)** Immunohistochemical staining of phosphorylated Akt (p-Akt; Ser473), pan-Akt, TH, HuC, and Synaptophysin (Synap) of the sagittal sections through IRG of a control mCherry transgenic fish (A–E), a myr-Akt2 fish with ganglioneuroma (F–J), and a MYCN fish with neuroblastoma (K–O). Arrows indicate head kidney. HK, head kidney; pNT, peripheral neuroblastic tumors. Scale bars, 20 µm. **(P–X)** Immunohistochemical staining of phosphorylated mTOR (p-mTOR; Ser2448), phosphorylated S6 ribosomal protein (p-S6; Ser235/236) and phosphorylated EIF4EBP1 (p-EIF4EBP1; Thr37/46) of the sagittal sections through IRG of mCherry transgenic line (P–R), myr-Akt2 line with ganglioneuroma (S–U), and MYCN line with neuroblastoma (V–X). Arrows indicate head kidney. Arrowheads indicate renal tubules. Scale bars, 20 µm.

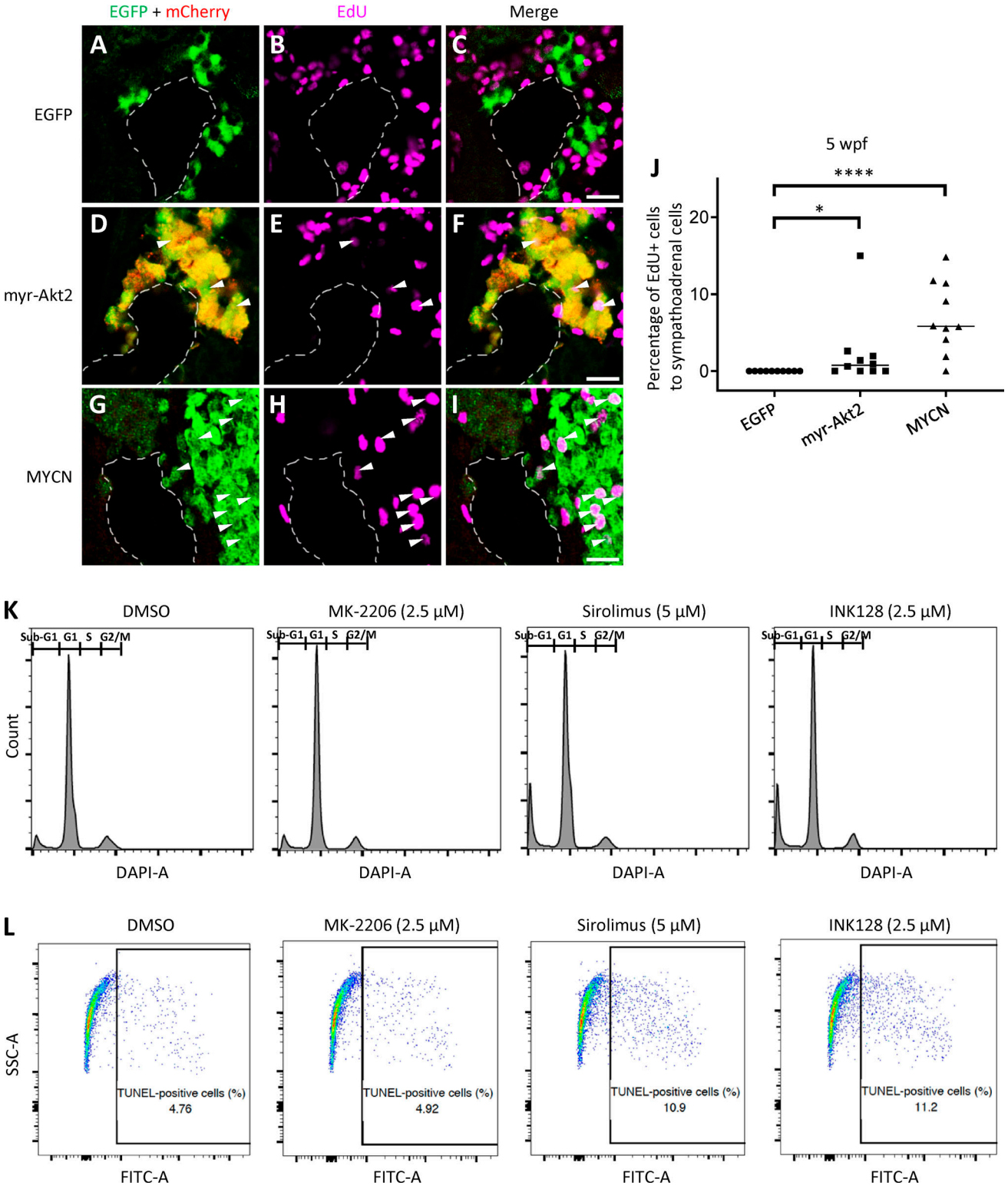

Figure S3. **Cellular phenotype of the sympathoadrenal lineage in the IRG of myr-Akt2 fish and flow cytometry analysis of zebrafish primary ganglioneuroma cells. (A–I)** Coimmunostaining of EGFP, mCherry and EdU of the sagittal sections through IRG of EdU-labeled EGFP (A–C), myr-Akt2;EGFP (D–F), and MYCN;EGFP (G–I) transgenic lines at 5 wpf. Arrowheads indicate the EdU-labeled proliferating sympathoadrenal cells. Dotted lines indicate the head kidney (HK) boundary. Scale bar, 20 μm. **(J)** Percentage of EdU-positive sympathoadrenal cells in the IRG of transgenic fish lines were plotted at 5 wpf. Each symbol represents the value for an individual fish. Horizontal bars indicate medians that were compared with two-tailed Wilcoxon rank-sum test. *, $P < 0.05$; ****, $P < 0.0001$. **(K and L)** Zebrafish primary ganglioneuroma cells were treated with the indicated compound for 48 h. Representative flow cytometric determinations are shown of cell cycle analysis after DAPI staining (K) and apoptotic cell analysis after TUNEL staining (L). Data are representative of three independent experiments.

Three tables are provided online. Table S1 shows the demographic characteristics of patients included in this study. Table S2 shows the expression data of 4,321 orthologues in human and zebrafish ganglioneuroma and neuroblastoma. Table S3 shows the tumor characteristics of patients.